Pressure–temperature phase diagrams of some heavy fermion systems

2007 J. Phys.: Condens. Matter 19 125205

(http://iopscience.iop.org/0953-8984/19/12/125205)

IOP PUBLISHING JOURNAL OF PHYSICS: CONDENSED MATTER

J. Phys.: Condens. Matter **19** (2007) 125205 (9pp) doi:10.1088/0953-8984/19/12/125205

Pressure–temperature phase diagrams of some heavy fermion systems

T C Kobayashi[1,2], H Hidaka[1,2], T Fujiwara[2], M Tanaka[2], K Takeda[2,3], T Akazawa[2,4], K Shimizu[2], S Kirita[5], R Asai[5], H Nakawaki[5], M Nakashima[5], R Settai[5], E Yamamoto[6], Y Haga[6] and Y Ōnuki[5,6]

[1] Faculty of Science, Okayama University, Okayama 700-8530, Japan
[2] KYOKUGEN, Osaka University, Toyonaka, Osaka 560-8531, Japan
[3] Faculty of Science and Engineering, Tokyo University of Science, Yamaguchi, Onoda 756-0884, Japan
[4] Faculty of Maritime Science, Kobe University, Kobe 658-0072, Japan
[5] Graduate School of Science, Osaka University, Toyonaka, Osaka 560-0043, Japan
[6] Advanced Science Research Centre, Japan Atomic Energy Research Institute, Tokai, Ibaraki 319-1195, Japan

E-mail: kobayashi@science.okayama-u.ac.jp

Received 3 January 2007
Published 6 March 2007
Online at stacks.iop.org/JPhysCM/19/125205

Abstract

We have studied the pressure–temperature phase diagrams in UIr, U_3P_4, UP_2, $CeAgSb_2$ and $CeMg_2Cu_9$ by means of the electrical resistivity. Application of pressure suppresses the magnetic ordering shown at ambient pressure in all compounds. In UIr, the pressure-induced superconductivity is observed in the vicinity of the magnetic–nonmagnetic transition. In this article, we review the pressure–temperature phase diagram and the properties of the magnetic–nonmagnetic transition in these compounds.

1. Introduction

Pressure-induced magnetic–nonmagnetic transition and the superconductivity near the critical pressure are among current topics of interest in condensed matter physics. In the last decade, pressure-induced superconductivity has been found in several Ce or U compounds, where a magnetically mediated mechanism due to the critical fluctuation was suggested. These compounds showed various pressure–temperature (P–T) phase diagrams as follows.

In $CeIn_3$, $CePd_2Si_2$ [1] and $CeRh_2Si_2$ [2, 3], the superconductivity appears only in the narrow pressure range near the antiferromagnetic–nonmagnetic critical point. The non-Fermi liquid (NFL) behaviour in the low temperature part of the resistivity in $CeIn_3$ and $CePd_2Si_2$ suggests the existence of critical fluctuation related to the appearance of superconductivity while the absence of NFL behaviour in $CeRh_2Si_2$ may suggest a different mechanism of superconductivity. On the other hand, in the cases of $CeCu_2Ge_2$ [4] and

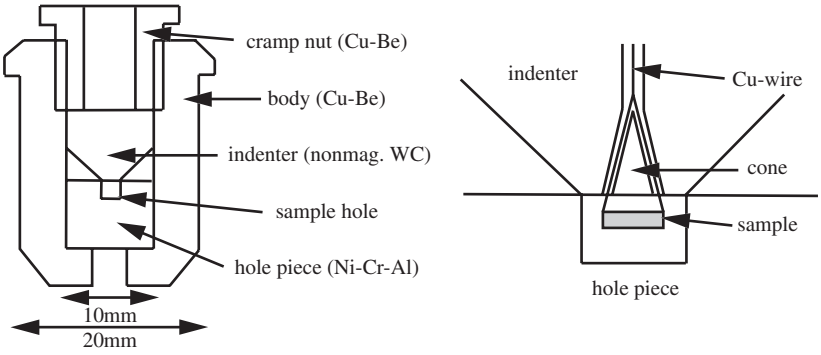

Figure 1. Indenter high pressure cell designed for low temperature and high field experiment.

$CeRhIn_5$ [5], the superconductivity can be observed in a relatively wide pressure range above the antiferromagnetic–nonmagnetic critical point. Correspondingly, the NFL behaviour is observed in the wide pressure range. The P–T phase diagram of $CeCu_2Ge_2$ has a characteristic enhancement of the superconducting transition temperature T_{SC}, which is also observed for $CeCu_2Si_2$. Another mechanism may be required to explain the enhancement of T_{SC} [6]. In some of compounds, the details of the P–T phase diagram, in particular the coexistence of antiferromagnetic ordering and superconductivity, are investigated microscopically by means of NMR [7, 8]. Recently the coexistence of superconductivity and ferromagnetic ordering has been discovered successively in UGe_2 [9, 10], URhGe [11] and $ZrZn_2$ [12]. In UGe_2, the superconductivity appears near P_C^* where a successive magnetic transition at T^* disappears. In UGe_2, the low temperature resistivity obeys the Fermi liquid form of T^2 near P_C^* and P_C where the ferromagnetic ordering vanishes. In order to obtain further insights into the NFL effects near the magnetic–nonmagnetic transition and its relevance to the onset of superconductivity, we need further systematic studies on the heavy fermion magnets.

We have been investigating the P–T phase diagrams and searched for superconductivity in some f electron systems by means of the electrical resistivity. The pressure-induced magnetic–nonmagnetic transitions have not been reported for all compounds. Application of pressure suppressed successfully the magnetic ordering in some of them. The pressure-induced superconductivity was found in UIr. In this article, we review the P–T phase diagram and the properties of the magnetic–nonmagnetic transition in these compounds.

2. Experiment

Pressure was applied by utilizing properly the indenter cell [13] and diamond anvil cell (DAC) according to the required pressure. The indenter cell shown in figure 1 was designed for the magnetic measurement which needed larger sample space than the DAC. The indenter made of nonmagnetic WC deforms the hole piece made of Ni–Cr–Al alloy by application of external force. The maximum pressure is about 5.0 GPa. The sample space has a diameter of 1.6 mm and initial height of about 1.4 mm which decreases with application of pressure. The pressure-transmitting medium was Daphne oil 7373 which has relatively low compressibility. The pressure value was estimated via the superconducting transition temperature T_{SC} of lead. The relation between T_{SC} and pressure was given by [14]. For higher pressure experiments on U_3P_4 and UP_2, the DAC has been used. The detail of preparation is described in [15]. The pressure-transmitting medium was Daphne oil 7373. The pressure value was determined through a shift

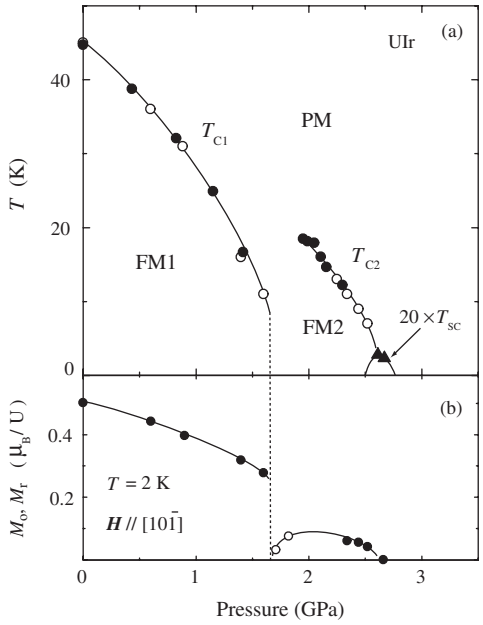

Figure 2. (a) P–T phase diagram of UIr. Solid and open circles are T_N determined by the resistivity and magnetization measurements, respectively. The superconductivity is observed near the critical pressure where the FM2 phase disappears. (b) Pressure dependence of the ordered moment along [1 0 $\bar{1}$] at 2 K. Solid circles are the ordered moments M_0 determined from the Arrott plot. Open circles are the residual magnetizations M_r.

in the R-line fluorescence spectrum of ruby. The electrical resistivity was measured by the conventional four-probe method. Magnetization measurement in UIr was carried out by using the conventional SQUID magnetometer. The high pressure cell for magnetization measurement is of indenter type, which will be reported on elsewhere.

3. UIr

UIr has the monoclinic PbBi-type structure without the inversion symmetry. The magnetic property at ambient pressure is Ising-like ferromagnetic with the Curie temperature $T_C = 46$ K [16]. The magnetic susceptibility follows the Curie–Weiss law with an effective moment $\mu_{eff} = 2.4\ \mu_B$/U while the ordered moment is 0.5 μ_B/U, indicating an itinerant nature of 5f electrons. The electrical resistivity measurement in a polycrystal of UIr under high pressures up to 1.86 GPa was reported, where the critical pressure for the suppression of ferromagnetism is estimated to be 4.0 GPa [17]. In this study, we used high quality single crystals which were grown by the Czochralski method in a tetra-arc furnace. The ingot was purified by a solid-state electrotransport method in a vacuum of 5×10^{-11} Torr. The residual resistivity ρ_0 and the residual resistivity ratio RRR ($= \rho_{RT}/\rho_0$) were 0.44 $\mu\Omega$ cm and 250, respectively, at ambient pressure.

The pressure–temperature phase diagram of UIr consists of a low pressure ferromagnetic phase FM1, a high pressure magnetic phase FM2 and a superconducting phase as shown in figure 2(a) [18]. Curie temperatures defined as T_{C1} (FM1) and T_{C2} (FM2) are determined by means of the resistance and magnetization measurements. The FM1 phase disappears abruptly at the critical pressure $P_{C1} \sim 1.7$ GPa and another magnetic phase FM2 with a

small ferromagnetic moment appears. The FM2 phase disappears at $P_{C2} \sim 2.6$ GPa. The novel superconductivity is observed in the narrow pressure range near P_{C2}, indicating that the superconductivity is due to the critical fluctuation associated with the disappearance of FM2 phase.

The pressure variation of the ordered moment M_0 at 2 K is shown in figure 2(b), where the external field is applied parallel to the [1 0 $\bar{1}$] direction which is the spin easy axis at ambient pressure. The ordered moment M_0 is estimated from an Arrott plot of the magnetization process. The ordered moment, which is 0.5 μ_B/U at ambient pressure, decreases with increasing pressure and reaches 0.28 μ_B/U at 1.6 GPa just below P_{C1}, and then decreases abruptly at $P_{C1} \sim 1.7$ GPa. Correspondingly, the magnetization process in $P_{C1} < P < 1.9$ GPa shows metamagnetic-like behaviour. The discrete change of the ordered moment and the metamagnetic-like behaviour indicate that the FM1–FM2 transition is of first order. In the FM2 phase, the ferromagnetic ordered moment along [1 0 $\bar{1}$] is smaller than that in FM1 phase. The maximum value of M_0 is 0.07 μ_B/U. At 2.6 GPa, the disappearance of the ordered moment is confirmed at 2 K. The absence of metamagnetic behaviour in $P > P_{C2}$ reveals that the FM2–nonmagnetic transition is of second order in contrast to the FM1–FM2 transition.

The superconductivity can be observed in the narrow pressure range of 2.61 GPa $< P <$ 2.65 GPa near P_{C2}. The superconducting transition temperature is 0.14 K at 2.61 GPa. The upper critical field H_{C2} at zero temperature is estimated to be about 26 mT. The temperature dependence of the resistivity obeys the non-Fermi liquid form of $T^{1.6}$ over the wide temperature range of 0.2 K $< T <$ 10 K, indicating that the critical fluctuation survives down to low temperatures. From these experimental facts, it is considered natural that the origin of the superconductivity is the critical fluctuation associated with the magnetic–nonmagnetic transition at P_{C2}.

The crystal structure of UIr lacks inversion symmetry. In the case of UGe_2 and URhGe, equal spin pairing is believed to occur in the superconducting state since the inversion symmetry guarantees the degeneracy of $|\mathbf{k}, \uparrow\rangle$ and $|-\mathbf{k}, \uparrow\rangle$ states. On the other hand, in the case of MnSi, the absence of superconductivity is believed to be due to the lack of inversion symmetry [9]. For UIr, it is still not clear whether the superconductivity coexists with the magnetic ordering or not. In the paramagnetic state outside of the FM2 phase, the electron system has time reversal symmetry, which guarantees the degeneracy of $|\mathbf{k}, \uparrow\rangle$ and $|-\mathbf{k}, \downarrow\rangle$ states. For the FM2 phase, time reversal symmetry is not expected any longer. The FM2 phase may not be simple ferromagnet and then the singlet pairing of $|\mathbf{k}, \uparrow\rangle$ and $|-\mathbf{k}, \downarrow\rangle$ may exhibit superconductivity due to the antiferromagnetic fluctuation. In order to investigate the magnetic properties of the FM2 phase, the magnetization measurements for other directions are now in progress.

4. U_3P_4

U_3P_4 crystallizes in the body centred cubic (bcc) structure of Th_3P_4 type with a space group of $I\bar{4}3d$. This crystal structure also lacks inversion symmetry. U_3P_4 is a ferromagnet with the Curie temperature $T_C = 138$ K at ambient pressure [19]. The magnetic susceptibility follows the Curie–Weiss law with an effective moment $\mu_{eff} = 2.75$ μ_B/U [20] while the ordered moment is obtained as 1.34 μ_B/U from the neutron scattering experiment [21], indicating the itinerant nature of 5f electrons. The magnetic structure is the non-collinear, three-sublattice magnetic structure with a ferromagnetic component along the [1 1 1] direction [21, 22]. The pressure effects on resistivity have been reported, where the application of pressure up to 8.2 kbar reduces T_C to 121.8 K [23]. A single crystal of U_3P_4 was prepared by the chemical transport method [19]. The residual resistivity ratio ρ_{RT}/ρ_0 reaches about 1500 in a single crystal used in the present study, indicating excellent quality.

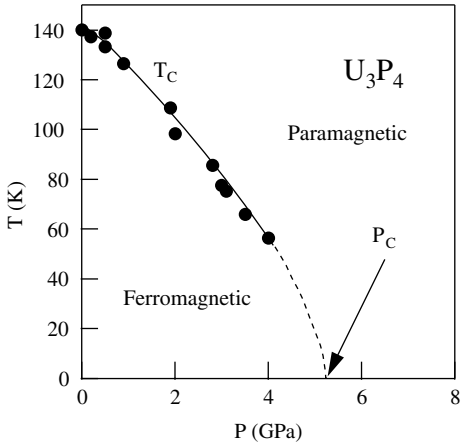

Figure 3. P–T phase diagram of U_3P_4. The critical pressure P_C of the ferromagnetic–nonmagnetic transition is determined by the pressure dependence of coefficient A of $\rho \sim AT^2$.

The pressure–temperature phase diagram of U_3P_4 is shown in figure 3. The temperature dependence of the resistivity increases slightly just below T_C and decreases with a upward curvature below T_C at ambient pressure. The Curie temperatures in figure 3 are defined as minima of $d\rho/dT$. Above 4.3 GPa the Curie temperature cannot be determined because the minimum of $d\rho/dT$ smears out. The critical pressure of the magnetic–nonmagnetic transition is determined as 5.0 GPa $< P_C <$ 5.3 GPa from the consideration of Fermi liquid behaviour $\rho(T) \sim AT^2$. The coefficient A determined at the low temperature limit shows a peak at 5.3 GPa. Moreover the temperature dependence of the resistivity at 5.0 GPa is close to $T^{5/3}$ predicted by the SCR theory in the case of three-dimensional ferromagnet [24]. In the case of MnSi, the NFL behaviours of $\rho \sim T^{3/2}$ near P_C were reported, where it was concluded that the origin of the $T^{3/2}$ law may lie in extremely subtle effects of disorder in the highest purity sample [25]. The NFL behaviour of $\rho \sim T^{1.6}$ near P_C was observed in another weak ferromagnet $ZrZn_2$ [12]. The $T^{5/3}$ law observed in U_3P_4 may be characteristic of the sample with excellent quality. More detail of the experimental data has been published in [26].

In the present study, no trace of superconductivity is observed in the pressure range up to 5.8 GPa and the temperature range down to 50 mK in spite of the excellent quality (RRR $\sim$ 1500). Its Th_3P_4 type crystal structure without the inversion symmetry may cause the absence of superconductivity, as indicated in the section on UIr.

5. UP_2

UP_2 has the tetragonal structure with the symmetry group $I4mm$, $a = 5.38$ Å and $c = 15.56$ Å [27]. UP_2 is an antiferromagnet with $T_N = 204$ K at ambient pressure. The magnetic susceptibility follows the Curie–Weiss law with an effective moment $\mu_{eff} = 2.29\ \mu_B$/U while the ordered moment is obtained as 2.0 μ_B/U from the neutron scattering experiment. The ordered moments parallel to the [0 0 1] direction form ferromagnetic (0 0 1) planes stacked along the [0 0 1] direction in an antiferromagnetic sequence (↑, ↓, ↓, ↑). The Shubnikov–de Haas effect measurement revealed that the cylindrical Fermi surfaces are formed in the flattened Brillouin zone due to the long unit cell along [0 0 1] and the conduction electrons are confined mainly in the U planes. In this study, we used a single crystal with excellent quality. The single-crystal samples were prepared by the chemical transport method [27]. The

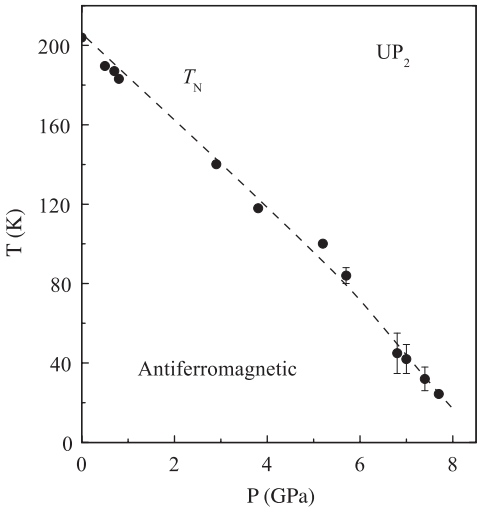

Figure 4. P–T phase diagram of UP_2. The critical pressure of the antiferromagnetic–nonmagnetic transition is estimated as $P_C \sim 8.5$ GPa from the extrapolation of T_N.

residual resistivity and the residual resistivity ratio are reported as $\rho_0 = 0.11$ $\mu\Omega$ cm and $\rho_{RT}/\rho_0 = 2900$, respectively.

The pressure–temperature phase diagram of UP_2 is shown in figure 4. The Néel temperature T_N is defined from a kink in the temperature dependence of the resistivity. Application of pressure reduces T_N monotonically up to 7.7 GPa which is the maximum pressure to date. The critical pressure of the magnetic–nonmagnetic transition is estimated as $P_C \sim 8.5$ GPa from extrapolation of the present data. UP_2 may be a good candidate for showing unconventional superconductivity in terms of the characteristic 2D Fermi surface and the 2D ferromagnetic correlation. A further experiment under higher pressure is required in order to search the superconductivity.

6. $CeAgSb_2$

$CeAgSb_2$ has tetragonal structure with the stacking of CeSb–Ag_2–CeSb–Sb_2 layers. Reflecting the quasi-two-dimensional electronic state, the resistivity is highly anisotropic: the resistivity for $J \parallel [0\ 0\ 1]$ is higher than that for $J \parallel [1\ 0\ 0]$ [28]. $CeAgSb_2$ shows the ferromagnetic ordering at $T_C = 9.7$ K. The ordered moments of 0.41 μ_B/Ce orient along the c axis. The magnetic moment is known to be well localized. Recently, the anisotropic magnetic behaviour has been explained in terms of the crystal electric field level scheme with the anisotropic exchange interaction [29, 30]. A single crystal grown by the self-flux method was used in the present experiment. The measuring current conducts in the c plane.

The pressure–temperature phase diagram of $CeAgSb_2$ is shown in figure 5(a). The ordering temperature is defined as a kink of the resistivity. Application of pressure decreases T_C and then the ordered state vanishes abruptly at $P_C = 3.3$ GPa. An important finding is the huge enhancement of the residual resistivity above P_C. The pressure dependence of the residual resistivity is shown in figure 5(b). The residual resistivity above P_C is about 50 $\mu\Omega$ cm which is much larger than that of 0.5 $\mu\Omega$ cm below P_C. It is confirmed that the residual resistivity reproduces the initial value when the pressure is released. The drastic change of electronic state may cause this anomalous behaviour. However, no drastic change is observed

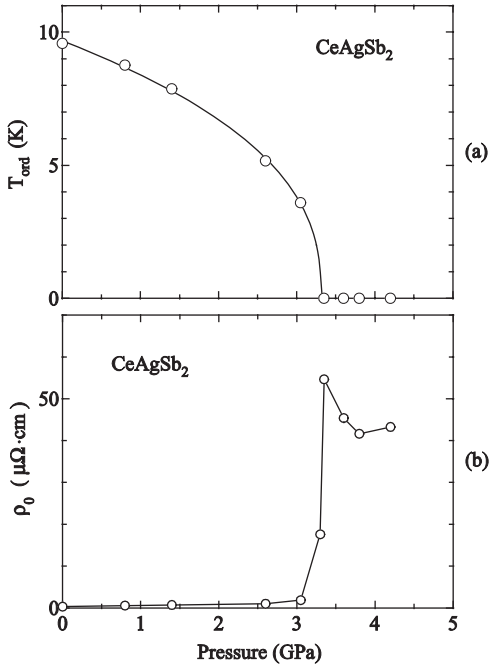

Figure 5. (a) P–T phase diagram of $CeAgSb_2$. (b) Pressure dependence of the residual resistivity. A huge enhancement is observed above P_C.

in the temperature dependence of the resistivity in the higher temperature region. No structural transition is confirmed at room temperature. Since the temperature dependence of the resistivity does not show the typical heavy fermion behaviour above P_C, further experiments are required in order to clarify the ground state above P_C. No sign of superconductivity is observed in the present experimental range of $T > 60$ mK and $P < 4.2$ GPa. More detail of the experimental results was described in [28].

7. $CeMg_2Cu_9$

The crystal structure of $CeMg_2Cu_9$ is hexagonal with the large lattice parameter c of 23.846 Å compared to the a value of 4.873 Å. The large lattice parameter c corresponds to a flat Brillouin zone, which is expected to bring about a two-dimensional electronic state. $CeMg_2Cu_9$ is antiferromagnet with $T_N = 2.7$ K. The effective magnetic moment of $\mu_{eff} = 2.43\ \mu_B$/Ce for $H \parallel [1\ 0\ \bar{1}\ 0]$ in the Curie–Weiss law is close to 2.54 μ_B for Ce^{3+}. The resistivity shows two broad maxima around 50 and 3 K just above T_N, which is due to a combination of the Kondo effect and the crystal electric field effect. In the present experiment, we used a single crystal grown by the slow cooling method: highly pure materials of Ce, Mg, and Cu were heated up to 1400 °C and cooled down slowly under an Ar atmosphere.

The pressure–temperature phase diagram of $CeMg_2Cu_9$ is shown in figure 6(a). The Néel temperature defined as a kink of resistivity shows weak pressure dependence at low pressures but then decreases drastically above 2 GPa. At 2.56 GPa no anomaly is observed and the coefficient A of the Fermi liquid form shows a peak. From these results, the critical pressure is determined as $P_C \sim 2.5$ GPa. The two maxima of resistivity at ambient pressure merge to one maximum at around P_C, which indicates that the crystal field splitting merges due to the c–f hybridization. This may be closely related to a steep decrease of T_N just

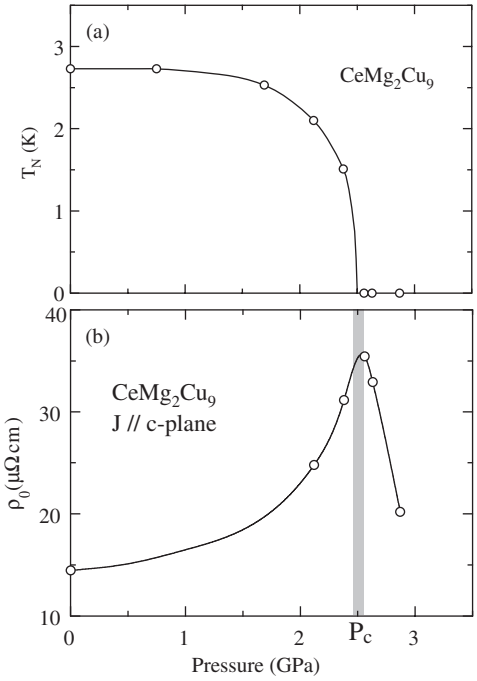

Figure 6. (a) P–T phase diagram of $CeMg_2Cu_9$. (b) Pressure dependence of the residual resistivity. Enhancement is observed near P_C.

below P_C. The resistivity maximum moves to higher temperature with further increasing pressure, corresponding to increase of the Kondo temperature. The enhancement of the residual resistivity ρ_0 at P_C is observed in $CeMg_2Cu_9$ as shown in figure 6(b). Though the enhancement of ρ_0 is observed in the case of ferromagnetic fluctuation as seen in MnSi, smaller enhancement is expected in the case of antiferromagnetic fluctuation.

No sign of superconductivity is observed in the present experimental range of $T > 90$ mK and $P < 2.83$ GPa. In this sample, the residual resistivity of 14 $\mu\Omega$ cm at ambient pressure is relatively large. The disorder in this sample might enhance the pair breaking effect of superconductivity. On the other hand, the abrupt disappearance of T_N and the absence of NFL behaviour may indicate a first-order antiferromagnetic–nonmagnetic transition. The absence of critical fluctuation may cause the disappearance of the superconductivity. More detail of the experimental results was described in [31].

8. Summary

Pressure-induced superconductivity is found in UIr without inversion symmetry. The superconductivity occurs in the vicinity of the magnetic–nonmagnetic transition. It is of interest how the superconductivity due to the magnetic fluctuation with the ferromagnetic component occurs in the compound without inversion symmetry where degeneracy of equal spin states with opposite momentum is not expected. In U_3P_4, the ferromagnetic–nonmagnetic transition is induced successfully, where the temperature dependence of resistivity is close to the non-Fermi liquid form of $T^{5/3}$ which is expected in the case of the ferromagnetic critical point. In UP_2, the antiferromagnetic ordering seems to be suppressed at around 8.5 GPa. For $CeAgSb_2$, a huge enhancement of residual resistivity ρ_0 is found above P_C. The residual resistivity of

$\rho_0 = 0.5\ \mu\Omega$ cm below P_C increases to $\rho_0 = 50\ \mu\Omega$ cm above P_C. A drastic change of the electronic state may cause this anomalous behaviour. For $CeMg_2Cu_9$, the enhancement of the residual resistivity is observed at the critical pressure of the antiferromagnetic–nonmagnetic transition, which cannot be explained by the antiferromagnetic fluctuation.

Acknowledgments

This work was supported by a Grant-in-Aid for Scientific Research COE (10CE2004) and Creative Scientific Research MEXT (15GS0123) from the Ministry of Education, Culture, Sports, Science and Technology of Japan.

References

[1] Matur N D, Grosche F M, Julian S R, Walker I R, Freye D M, Haselwimmer R K W and Lonzarich G G 2001 *Nature* **394** 39
[2] Movshovich R, Graf T, Mandrus D, Thompson J D, Smith J L and Fisk Z 1996 *Phys. Rev.* B **53** 8241
[3] Araki S, Nakashima M, Settai R, Kobayashi T C and Ōnuki Y 2002 *J. Phys.: Condens. Matter* **14** L377
[4] Jaccard D, Wilhelm H, Alami-Yadri K and Vargoz E 1999 *Physica* B **259–261** 1
[5] Hegger H, Petrovic C, Moshopoulou E G, Hundley M F, Sarrao J L, Fisk Z and Thompson J D 2000 *Phys. Rev. Lett.* **84** 4986
[6] Holmes A T, Jaccard D and Miyake K 2004 *Phys. Rev.* B **69** 24508
[7] Kitaoka Y, Ishida K, Kawasaki Y, Trovarelli O, Geibel C and Steglich F 2001 *J. Phys.: Condens. Matter* **13** L79
[8] Kawasaki S, Mito T, Kawasaki Y, Zheng G-q, Kitaoka Y, Aoki D, Haga Y and Ōnuki Y 2003 *Phys. Rev. Lett.* **91** 137001
[9] Saxena S S *et al* 2000 *Nature* **406** 587
[10] Huxley A, Sheikin I, Ressouche E, Kernavanois N, Braithwaite D, Calemczuk R and Flouquet J 2001 *Phys. Rev.* B **63** 144519
[11] Aoki D, Huxley A, Ressouche E, Braithwaite D, Flouquet J, Brison J-P, Lhotel E and Paulsen C 2001 *Nature* **413** 613
[12] Pfleiderer C, Uhlarz M, Hayden S M, Vollmer R, von Lohneysen H, Bernhoeft N R and Lonzarich G G 2001 *Nature* **412** 58
[13] Kobayashi T C, Hidaka H, Kotegawa H, Fujiwara K and Eremets M I 2007 *Rev. Sci. Instrum.* at press
[14] Bireckoven B and Wittig J 1988 *J. Phys. E: Sci. Instrum.* **21** 841
[15] Shimizu K, Kobayashi T C, Muramatsu T, Takeda K, Hashimoto K and Amaya K 1999 *Proc. AIRAPT-17* p 1089
[16] Yamamoto E, Haga Y, Matsuda T D, Nakamura A, Settai R, Inada Y, Sugawara H, Sato H and Ōnuki Y 2002 *J. Nucl. Sci. Technol.* **3** (Suppl.) 187
[17] Bauer E D, Freeman E J, Sirvent C and Maple M B 2001 *J. Phys.: Condens. Matter* **13** 5675
[18] Another phase boundary was found recently in this pressure–temperature phase diagram. FM2 denoted in this paper corresponds to FM3 in the following papers
Kobayashi T *et al* 2006 *Physica* B **378** 355
Hori A *et al* 2006 *J. Phys. Soc. Japan* **75** (Suppl.) 82
[19] Inada Y, Wisniewski P, Murakawa M, Aoki D, Miyake K, Watanabe N, Haga Y, Yamamoto E and Ōnuki Y 2001 *J. Phys. Soc. Japan* **70** 558
[20] Troc R, Mulak J and Suski W 1971 *Phys. Status Solidi* b **43** 147
[21] Wisniewski P, Gukasov A and Henkie Z 1999 *Phys. Rev.* B **60** 6242
[22] Burlet P, Rossat-Mignod J, Troc R and Henkie Z 1981 *Solid State Commun.* **39** 745
[23] Henkie Z 1980 *Phys. Status Solidi* a **58** K219
[24] Moriya T 1985 *Spin Fluctuations in Itinerant Electron Magnetism* (*Springer Series*) (Berlin: Springer)
[25] Pfleiderer C, Julian S R and Lonzarich G G 2001 *Nature* **414** 427
[26] Takeda K *et al* 2002 *J. Nucl. Sci. Technol.* **3** (Suppl.) 191
[27] Wisniewski P, Aoki D, Watanabe N, Settai R, Haga Y, Yamamoto E and Ōnuki Y 2001 *J. Phys. Soc. Japan* **70** 278
[28] Nakashima M *et al* 2003 *J. Phys.: Condens. Matter* **15** L111
[29] Takeuchi T *et al* 2003 *Phys. Rev.* B **67** 64403
[30] Araki S, Metoki N, Galatanu A, Yamamoto E, Thamizhavel A and Ōnuki Y 2003 *Phys. Rev.* B **68** 24408
[31] Nakawaki H *et al* 2002 *J. Phys.: Condens. Matter* **14** L305